Enhancement of giant magnetoresistance and oscillation by wave-vector filtering in Fe/Ag/Fe/InAs/Ag

Ziran Wang and R. H. Victora

Phys. Rev. B **94**, 245415 — Published 12 December 2016

DOI: 10.1103/PhysRevB.94.245415

GMR enhancement and oscillation by wave vector filtering in Fe/Ag/Fe/InAs/Ag

Ziran Wang[1] and R. H. Victora[1, 2, *]

[1] *School of Physics and Astronomy, University of Minnesota-Twin Cities, Minneapolis, Minnesota 55455 USA*
[2] *Department of Electrical Engineering, University of Minnesota-Twin Cities, Minneapolis, Minnesota 55455 USA*

(Dated: October 11, 2016)

The performance of a novel giant magnetoresistance (GMR) heterostructure Fe/Ag/Fe/InAs/Ag(100) in the current-perpendicular-to-plane geometry is presented. Calculations are based on a realistic tight-banding model with full *spd* bands and the recursive Green's function algorithm. Results show that the system's GMR can reach values above 1000%. This GMR enhancement mainly is a result of the wave vector filtering effect imposed by the InAs layer, restricting conductance within a small region around the Γ point in the 2D Brillouin Zone. Calculations also reveal that when the Fermi level sits in the InAs band gap, GMR gradually saturates as a function of InAs thickness with a smooth plateau; whereas when the Fermi level is in the InAs conduction band and close to the band bottom, GMR exhibits an oscillatory behavior with a large period. This GMR oscillation in a semiconductor sandwiched between a ferromagnetic layer and a nonmagnetic layer is a novel phenomenon that has never been reported before. GMR oscillations are also observed with respect to Ag thickness, with oscillation amplitude determined by the Fermi level position relative to the InAs conduction band edge. The oscillation periods in both cases can be well explained by the concept of quantum-well states, and are determined by the spanning vector of the Fermi surface belly of the material whose thickness is varied. The observed GMR oscillations are due to the quantum interference of conduction electrons near the Γ point. The GMR and area-resistance (RA) product profiles at a wide range of InAs Fermi energies are also compared. Near the GMR peak (with GMR above 1000%) in the conduction band, RA product can be as low as $8.8\,\Omega\,\mu m^2$. This feature of large GMR but small RA product results from the wave vector filtering effect of doped InAs, and it makes the structure under study distinct from conventional GMR systems (small GMR, small RA) or magnetic tunnel junctions (large GMR, large RA).

PACS numbers: 75.47.De, 73.40.Sx, 73.23.Ad, 73.40.Gk

I. INTRODUCTION

Since the discovery of giant magnetoresistance (GMR) in Fe/Cr multilayers by Fert[1] and Grünberg[2], GMR heterostructures have been widely applied in biotechnology as biosensors, in spintronics as building blocks of spin-transfer-torque random access memory, and in magnetic storage technology as read heads (although GMR sensors have not been recently used as read heads, there is an expected transition back to GMR sensors as areal densities of hard drives keep growing[3]). This motivates extensive research to understand its mechanism. It is now well understood that the spin-dependent scattering plays an important role in the mechanism of GMR effect, which has been demonstrated in experimental and theoretical works[4–7] for both current-in-plane (CIP) and current-perpendicular-to-plane (CPP) geometries. While the GMR effect was first discovered in the CIP geometry, GMR in the CPP geometry is usually much higher than CIP. Our work in this article mainly focuses on CPP GMR with clean interfaces.

Many new GMR heterostructures with various materials have also been explored by experiments, including Fe/Ag[8], Fe/Cu[9], Co/Cu[10], Co/Ru and Co/Cr[11]. Interestingly, in all of these systems, GMR and the exchange coupling between ferromagnetic layers are both found to oscillate with the thickness of nonmagnetic spacer. Moreover, the periods of both oscillations consistently coincide with each other[9–11], and GMR reaches its enhanced values when the exchange coupling is antiferromagnetic. It is believed that this oscillatory behavior of exchange coupling and GMR should be ascribed to the exchange interactions mediated by conduction electrons in the spacer[12]. While this interpretation strongly suggests a Ruderman-Kittel-Kasuya-Yosida(RKKY)-like interaction between the ferromagnetic layers, the experimental oscillation periods are often found to be much larger than the predictions from simple RYYK-like models. Numerous theoretical models have been proposed to explain this discrepancy[13–15]. The theory in Ref.[15] provides an especially insightful picture, where it utilizes the concept of quantum-well state and its modulation on top of the Bloch waves to give a universal explanation of the magnetic coupling oscillation in various multilayer structures. It turns out that this interpretation is equivalent to a theoretical treatment where the RKKY coupling is evaluated in a superlattice with discrete lattice spacing. The resulting equation to calculate the oscillation period suggests that the period is determined solely by the band structure of the nonmagnetic spacer, and the values of the periods obtained from it are quantitatively consistent with experiments. This quantum-well model of GMR oscillation also appears to be applicable to our simulation results presented later in this paper.

In many applications, there are requirements not only on the magnetoresistance (MR) of the device, but also

the total resistance. Both MR and the total resistance control the signal-to-noise ratio of a device, and the total resistance also determines the amplitude of the signal that the device can produce. However, the magnitude of GMR in known structures is very small, usually around the order of 10%∼100% even at low temperatures. Moreover, in order to produce a detectable signal, GMR devices often need to adopt a nanopillar structure because of the relatively small resistances of its metallic components. This low MR and low resistance feature appears in every conventional GMR structure, significantly limiting its application, for example, in high areal density magnetic recording.

On the other hand, instead of a metallic nonmagnetic spacer, one can insert an insulator between the ferromagnetic layers, and form a magnetic tunnel junction (MTJ). The tunneling magnetoresistance (TMR) of MTJ is usually higher than its GMR counterpart. A TMR of 30% at 4.2K and 18% at room temperature was observed in $Fe/Al_2O_3/Fe$ junctions[16]. Later, Butler[17] and Mathon[18] independently made the theoretical prediction that in a fully crystalline Fe/MgO/Fe junction the TMR can reach the order of 1000%. This prediction has been confirmed by experiments[19,20], where TMR up to 200% at room temperature was observed, and a TMR of 1100% has been reported in a CoFeB/MgO/CoFeB junction[21]. The fact that the experimental value of TMR is approaching its theoretical prediction gives a strong proof of the validity of the theoretical models. Both models (Butler's and Mathon's) suggest that there are two main ingredients in the emergence of a large TMR: (a) coherent tunneling of highly spin-polarized Δ_1 Bloch states (symmetry filtering), and (b) tunneling in the direction of in-plane wave vector $k_{||} \approx 0$ (wave vector filtering towards the Γ point). The Δ_1 states are polarized because they decay at a slower rate in MgO than states with other symmetries and these states are only available to the majority spin of Fe. This asymmetry between transport of majority and minority spins is the strongest at the center of the 2D Brillouin Zone (Γ point). Therefore, a thick MgO barrier that strongly favors perpendicular tunneling can ensure the selection of electrons near the Γ point and increases the TMR. However, the necessity of a thick insulating MgO raises a disadvantage in these TMR structures: high MR can only be achieved with high resistance, which causes impedance mismatch to the preamplifier, decreases the speed of the device, and increases its energy consumption. In fact, the resistance-area (RA) product of an MgO junction is typically many orders of magnitude larger than that of a conventional metallic GMR structure, and thus scales poorly with decreasing device size.

Given that both conventional GMR and TMR structures suffer from shortcomings, a heterostructure that can exhibit high MR while maintaining a small resistance, or even a tunable resistance, is therefore very desirable. A reasonable question to ask is, by applying the above physics of large TMR in MgO junctions, whether

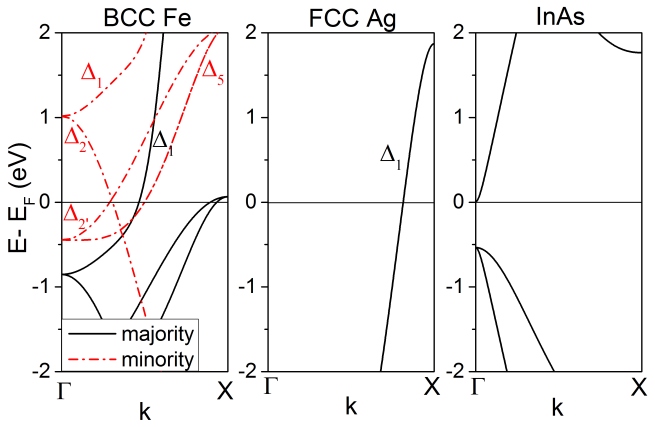

FIG. 1. Band structures of Fe, Ag and InAs (lightly doped) in (100) direction.

the GMR of a fully metallic heterostructure can be engineered to be as large as, or even larger than, the MgO junctions' TMR. The authors of[22] have provided a possible answer to this question. They proposed a structure with a conventional GMR trilayer Fe/Ag/Fe attached to a lightly doped InAs substrate, and showed that it could exhibit GMR up to 10^5% at zero temperature with clean interfaces. Since the Δ_1 states are only available in the majority spins of Fe, and the Fermi level only meets with the Δ_1 band in Ag, the Fe/Ag interface serves as a symmetry filter and polarizes the Δ_1 electrons. Unlike Fe/MgO junctions, here the wave vector filtering effect is no longer a result of a thick insulating spacer, but due to the fact that the Fermi surface of a lightly doped InAs can be engineered to be very small surrounding the Γ point. Since propagating modes are available throughout the Fe/Ag/Fe/InAs structure in this case, the resistance is expected to be small. Moreover, the resistance can be tuned because the Fermi surface of InAs can be altered by its doping level. The above statements about the band structures in Fe/Ag/Fe/InAs is illustrated in Fig. 1.

While this ultra-high GMR in Fe/Ag/Fe/InAs is very appealing, in practical applications the InAs layers are likely to be terminated by other materials. With a finite length of the InAs collimator and the introduction of an additional interface, the GMR may be well below the above predicted value and could exhibit other interesting behaviors. To explore these speculations, we study the GMR as a function of the InAs collimator thickness and the Ag spacer thickness at various InAs Fermi energies. In order to terminate the InAs layers while maintaining the band structure matching in the system, we choose to use Ag as one of the semi-infinite leads, as shown in the schematic picture of the heterostructure Fe/Ag/Fe/InAs/Ag(100) under study (Fig. 2). Note that the FCC lattice of Ag needs to rotate 45° to match the BCC lattice of Fe and the zinc blende lattice of InAs. Given the lattice constant of Fe $a_{Fe} = 2.87\mathring{A}$, we see

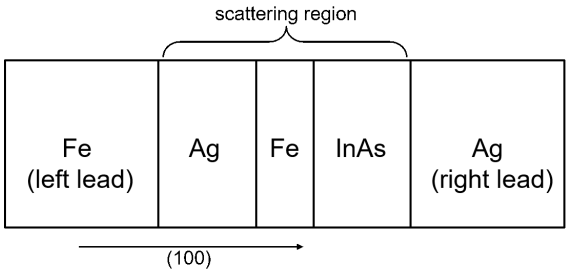

FIG. 2. Schematic picture of the system under study.

that the lattice constant of InAs ($6.05\mathring{A}$) is close to $2a_{Fe}$ and the lattice constant of Ag ($4.09\mathring{A}$) close to $\sqrt{2}a_{Fe}$. Therefore, we assume a perfect lattice match throughout the system during our calculations. We also assume that the Fermi levels of all layers align with each other, and according to experiments[23], no Schottky barrier is formed at the Fe/InAs interface. Defining the top of the InAs valance band to be zero energy, the Fermi level position relative to the InAs conduction band edge is selected to represent different doping levels, which can be determined by the dopant density through the parabolic band formula $n = 2\sqrt{2(mE_f)^3}/3\hbar^3\pi^3$, where n is the electron density and m is the effective mass. We assume that the Fermi level position is spatially uniform. This assumption is simplifying, because the Fermi level pinning[24] and band bending effects near the InAs interfaces are ignored. However, since the energy difference between the pinned Fermi level and the conduction band edge at the interface is very small, usually less than 0.1eV according to experiments[25] (the exact value or even the sign of this energy difference is not yet very clear[25–27]), most of our calculations with thick InAs layers take place where the Fermi level varies slowly with spatial position. We therefore believe that our assumption would not cause qualitative errors. This assumption has been checked in the realistic case of $5 \times 10^{17}\text{cm}^{-3}$ electron density and energy offset at the interface of 0.04eV by solving the Poisson equation and adjusting the on-site energies as functions of varying overall InAs thickness. A GMR of about 2000% and an oscillation period of about 80 monolayers is produced, in quite close agreement to our simplified approach for the same Fermi level (an electron density of $5 \times 10^{17}\text{cm}^{-3}$ corresponds to a Fermi level 0.1eV above the InAs conduction band edge from the parabolic band approximation). The corresponding GMR from our simplified approach is also about 2000% and the oscillation period is also about 80 monolayers, see Fig. 4 and Table. I later in this paper.

In the following sections of this article, we will first describe our theoretical model and computational approach towards a realistic simulation for the transport properties of Fe/Ag/Fe/InAs/Ag. Then we will move on to examine our simulation results and study the GMR dependence on InAs thickness, Ag thickness and the Fermi level position.

II. SIMULATION METHODS

A. Tight-binding model and Fisher-Lee relation

We start our calculations by constructing our system's Hamiltonian based on a tight-binding model. For each spin, the general form of the Hamiltonian reads:

$$H = \begin{bmatrix} H_L & T_{L,1} & & & & & \\ T_{1,L} & H_1 & T_{1,2} & & & & \\ & T_{2,1} & H_2 & & & & \\ & & & \ddots & T_{N-1,N} & & \\ & & & T_{1,N-1} & T_N & T_{N,R} & \\ & & & & T_{R,N} & H_R & \end{bmatrix}. \quad (1)$$

Here, N is the total number of atomic layers in the scattering region. $H_i\,(i = 1 \ldots N)$ represents the on-site Hamiltonian of layer i. H_L and H_R represent the Hamiltonian of the left and right semi-infinite leads respectively. The elements $T_{i,j}$'s are the hopping matrices connecting layer i to layer j, because only nearest-neighbor interactions are considered, only the $T_{i,j}$'s that relate nearest layers are nonzero. Notice that each matrix element mentioned above is by itself also a matrix. The dimension of these sub-matrices is $N_{orb}M \times N_{orb}M$, which is determined by the number of atomic orbitals N_{orb} and the number of atoms M on each layer. We have included full *spd* orbitals for Fe, Ag and InAs, thus $N_{orb} = 9$. Each layer consists of 2 atoms with periodic boundary condition, i.e. $M = 2$. The Slater-Koster parameters used to calculate the Hamiltonian matrix elements are taken from Ref.[28] for Fe and Ag. It needs to be pointed out that the parameters from Ref.[28] were derived with next-to-nearest neighbor interactions, while we only use the nearest neighbor parameters in our simulations. This will cause slight distortion of the bands, particularly the *s-p* bands, but since the symmetries and overall positions of the bands are unchanged, the distortion is unlikely to bring about qualitatively different results. The Slater-Koster parameters for the InAs *spd* orbitals are obtained by a nonlinear least squares fitting to the *spds** bands given in Ref.[29]. Because of the lack of the s^* orbital that is important for the exact shape of the conduction band, our fitted results are only valid within some tenths of eV above the conduction band bottom (with a 0.05eV difference of the band gap compared to Ref.[30]). However, since the wave vector filtering effect that we are interested in occurs only when the Fermi level is close to the band bottom, we believe that our fitted parameters for InAs are realistic enough for the purpose of this article, and will not cause any qualitative errors. The hopping parameters between layers of different materials are calculated by Harrison's formula[30].

In order to study the magnetoresistance of the system, we use the Fisher-Lee formula[31] to relate the conductance G with the transmission coefficients of the electrons:

$$G = \frac{e^2}{h} Tr(t^+ t) = \sum_{k,k',\sigma} t^{\sigma}_{k,k'} t^{\sigma *}_{k,k'}, \quad (2)$$

where the sum is over the 2D Brillouin Zone perpendicular to the (100) direction, and $t^{\sigma}_{k,k'}$ is the transmission coefficient of an incoming wave with transverse wave vector k transmitted to an outgoing wave at k' for a spin channel σ. The GMR is then defined as GMR $= (G_P - G_{AP})/G_{AP}$, where G_P is the conductance when the magnetizations of Fe are parallel (P) and G_{AP} is the conductance when the magnetizations are antiparallel (AP).

The transmission coefficients can be extracted from the Green's function of the system, using the general Green's function formalism proposed by Ref.[32]:

$$t_{k_R,k_L} = \widetilde{\Phi}^{+}_{k_R} G(k_L, k_R) \mathcal{V} \Phi_{k_L} \sqrt{\frac{v_{k_R}}{v_{k_L}}} e^{-ik_R D}. \qquad (3)$$

Here, $G(k_L, k_R)$ is the Green's function matrix element that connects the perpendicular wave vector k_L in the left lead to k_R in the right lead. $v_{k_L}(v_{k_R})$ is the group velocity of the propagating mode in the left (right) lead with wave vector $k_L(k_R)$. Φ_{k_L} and Φ_{k_R} represent the set of eigenvectors of the Schrödinger equation for the leads. $\widetilde{\Phi}^{+}$ is the corresponding inverse of Φ with $\widetilde{\Phi}^{+}_{k}\Phi_{k'} = \delta_{k,k'}$. $\mathcal{V}$ is a complicated matrix constructed from Φ, $\widetilde{\Phi}^{+}$ and the hopping matrices of the leads, its definition can be found in Ref.[32]. D is the length of the scattering region. We will dedicate the next section to the method of calculating $G(k_L, k_R)$. The evaluation of the other quantities needed on the right hand side of Eq. (3) depends on solving the Schrödinger equation of the semi-infinite leads: detailed description of the method can be found in Ref.[33].

B. Recursive Green's function algorithm

From the above discussion, we have seen that the central link between the Hamiltonian and the conductance of the system is the Green's function element $G(k_L, k_R)$ that connects the leads. Consider a structure with $M \times M$ atoms on one atomic plane and with N planes in the scattering region. Naively, in order to obtain the complete Green's function (and thus the element $G(k_L, k_R)$), we can directly invert the whole $M^2N \times M^2N$ Hamiltonian matrix, which typically has a time complexity of $O(M^6N^3)$. Owing to the strong k-space filtering effect present in Fe/Ag/Fe/InAs/Ag, conduction occurs only in a small region of the 2D Brillouin Zone, and to achieve convergence, about 10^6 k-points need to be sampled. Thus, direct inversion of the Hamiltonian will be too computationally expensive. To see this, notice the Green's function calculated this way is redundantly expensive, because only the matrix elements that connects the leads are used in equation (3). Alternatively, instead of dealing with the system as a whole, we can add one atomic layer at a time and calculate only the necessary Green's function elements recursively. This way, we only need to invert a $M \times M$ matrix each time for N layers, which leads to a time complexity of $O(M^6N)$. Compared to the $O(M^6N^3)$ complexity of direct inversion, this recursive Green's function technique is especially efficient for systems with large N. In our study, N normally takes a value more than 100, and by applying the recursive Green's function algorithm, it implies more than 4 orders of magnitude acceleration. The foundation of this useful method was laid by Thouless and Kirkpatrick[34], and has become a standard tool to compute transport properties of various mesoscopic systems[35–39].

In all of the calculations presented in this article, the thickness of the second Fe layer is fixed to be 8 monolayers, and the variables are the InAs thickness, the Fermi level position relative to the InAs conduction band edge, and the Ag thickness. An imaginary part of 10^{-3}eV is added to the Fermi energy to ensure numerical stability. 10^6 k-points are sampled in the 2D Brillouin Zone. We have checked that doubling the mesh density gives an average error less than 5%, so the results are believed to have achieved convergence.

III. SIMULATION RESULTS

A. GMR dependence on InAs thickness

As explained in Section I, the enhancement of GMR in Fe/Ag/Fe/InAs/Ag is greatly due to the wave vector filtering effect imposed by InAs on the Fe/Ag/Fe trilayer, limiting electron transmission to a small region around the Γ point. Since this is a property of the Fermi surface of bulk InAs, when the thickness of InAs is decreased one could expect the wave vector filtering effect to be weakened and thus the GMR. Also, the position of Fermi level can alter the size of the InAs Fermi surface, this will change the GMR behavior as well. We thus start our discussion on the simulation results by looking into the GMR dependence on InAs thickness at different Fermi levels. Firstly, we fix the Ag spacer thickness to be 4 monolayers, and select two Fermi levels (0.27eV and 0.45eV) in the InAs band gap. The results are plotted in Fig. 3(a). In both cases, MR starts to increase dramatically with about 20 InAs monolayers (∼6nm), reaches 1000% with about 40 monolayers (∼12nm), and eventually arrives at a saturation plateau. The saturation behavior of MR here is very similar to the one of Fe/MgO MTJs with increasing MgO thickness[20]. Although, InAs in this case is actually an insulator, and serves as a k-space filter that favors perpendicular tunneling just as MgO does, it should be emphasized that the MR saturations in these two situations actually result from distinct mechanisms. As demonstrated in Ref.[40] by simulations, the MR saturation in Fe/MgO junctions occurs only when the interfaces are disordered (which must be the condition in the experiments of Ref.[20]), otherwise, MR would keep growing monotonically with increasing MgO thickness. Since we assume clean interfaces throughout our system, apparently the above explana-

tion doesn't apply. In fact, as mentioned in Section I, in Fe/MgO junctions, MgO is not only a wave vector filter (favoring electrons near the Γ point), but also a symmetry filter (favoring the Δ_1 states only in the majority spin). As a result, the conductance of P configuration keeps decaying at a slower rate than the conductance of AP configuration inside MgO, and this manifests as a monotonic MR growth without saturation. On the contrary, in our system Fe/Ag/Fe/InAs/Ag, InAs only serves as a wave vector filter, which means that inside InAs, the Δ_1 states in majority spin doesn't have an advantage in transmission over other states in minority spins. Therefore, the increase of MR with increasing InAs thickness only comes from restricting electron transmission towards the Γ point. Once the thickness of InAs is large enough, and basically only the electron at the Γ point can effectively transmit, MR will stop increasing because the conductance of P configuration now decays at a similar rate inside InAs as the conductance of AP configuration. This can also be understood by merely looking at the conductance contrast close to the Γ point of a Fe/Ag/Fe trilayer. Our simulations show that the conductance ratio between P and AP configuration near the Γ point is not infinite (although can be up to 10^7%). One can imagine that by imposing the wave vector filtering effect of InAs, the MR should be limited by this conductance ratio set by the Fe/Ag/Fe layers, and therefore should exhibit a saturation behavior. Owing to the small band gap of InAs, the enhancement of MR doesnt have to give rise to very large resistance as in MgO junctions. Fig. 3(b) shows the relation between MR and the RA product of P configuration for the same two cases. When the Fermi level is deep in the band gap (0.27eV), the RA product is much higher than when its close to the conduction band bottom. Nonetheless, to achieve an MR above 1000%, the RA product can be as low as about $10\,\Omega\,\mu m^2$. Considering the RA product of Fe/MgO MTJ is typically of the order of $1000\,\Omega\,\mu m^2$, our system clearly demonstrates the advantage of significantly smaller resistance with sufficiently enhanced MR.

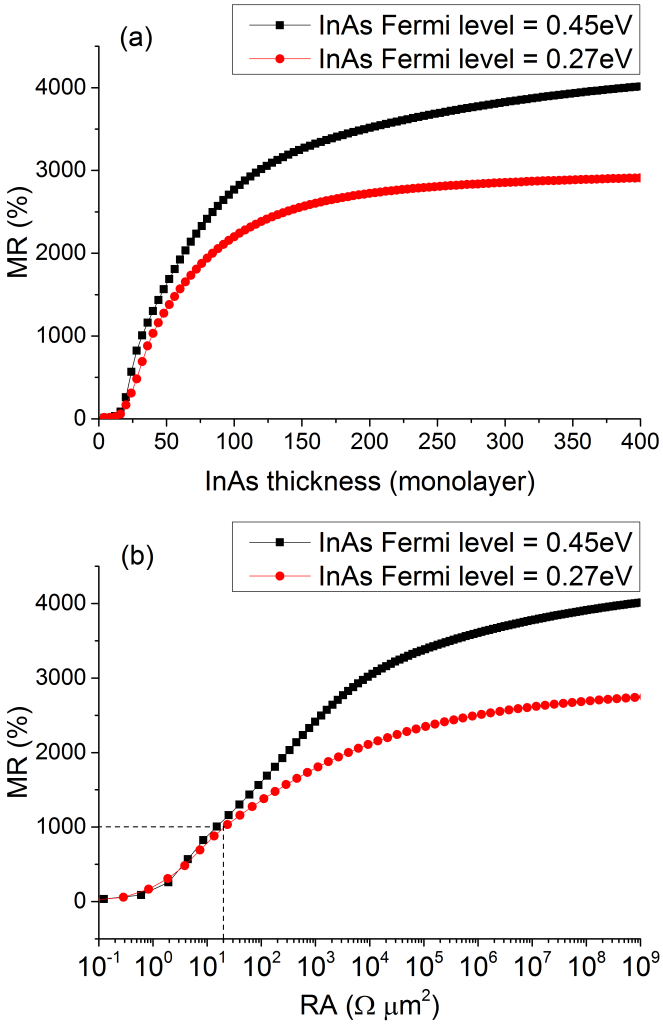

FIG. 3. MR dependence on the InAs thickness (a) and the relation between MR and RA of P configuration (b) when the Fermi level sits in the InAs band gap. The band gap of InAs is from 0eV to 0.47eV. The dashed lines are to indicate a GMR of 1000% with an RA product about $10\,\Omega\,\mu m^2$.

We now move on to study the GMR dependence on the InAs thickness when the Fermi level is in the InAs conduction band. Again we fix the Ag spacer thickness to be 4 monolayers, and select various Fermi energies ranging from 0.48eV to 0.57eV. The results are plotted in Fig. 4. Instead of the smooth saturation shown above, the GMR in these cases is an oscillatory function of InAs thickness. And the GMR tends to be smaller when the Fermi level is larger, because a larger Fermi level allows more electrons away from the Γ point to conduct and weakens the wave vector filtering effect. Clearly, whether the InAs Fermi level is positioned in the gap or in the conduction band draws a line between two distinct MR behaviors. This strongly indicates that the GMR oscillation is a result of the quantum interference of propagating modes that are available in InAs only when the Fermi energy is large enough to activate electrons in the conduction band. More interestingly, the oscillation period obviously correlates to the Fermi level position relative to the InAs conduction band edge: the larger the Fermi energy, the smaller the period. This correlation between the GMR oscillation period and the band structure of the conducting nonmagnetic layer is in fact a universal phenomenon that emerges in almost every GMR structure, as we mentioned earlier in Section I. Among many theoretical works to provide explanations to the periodicity in GMR, we find that the model in Ref.[15] is fairly simple, but can provide results that agree very well with experiments. Thus we will briefly describe its formalism below, and apply it to our simulation results in order to draw a quantitative relation between the Fermi level position and the GMR oscillation period. The model argues that the wave function in a heterostructure can be viewed as a quantum-well state consisting of a Bloch function that is

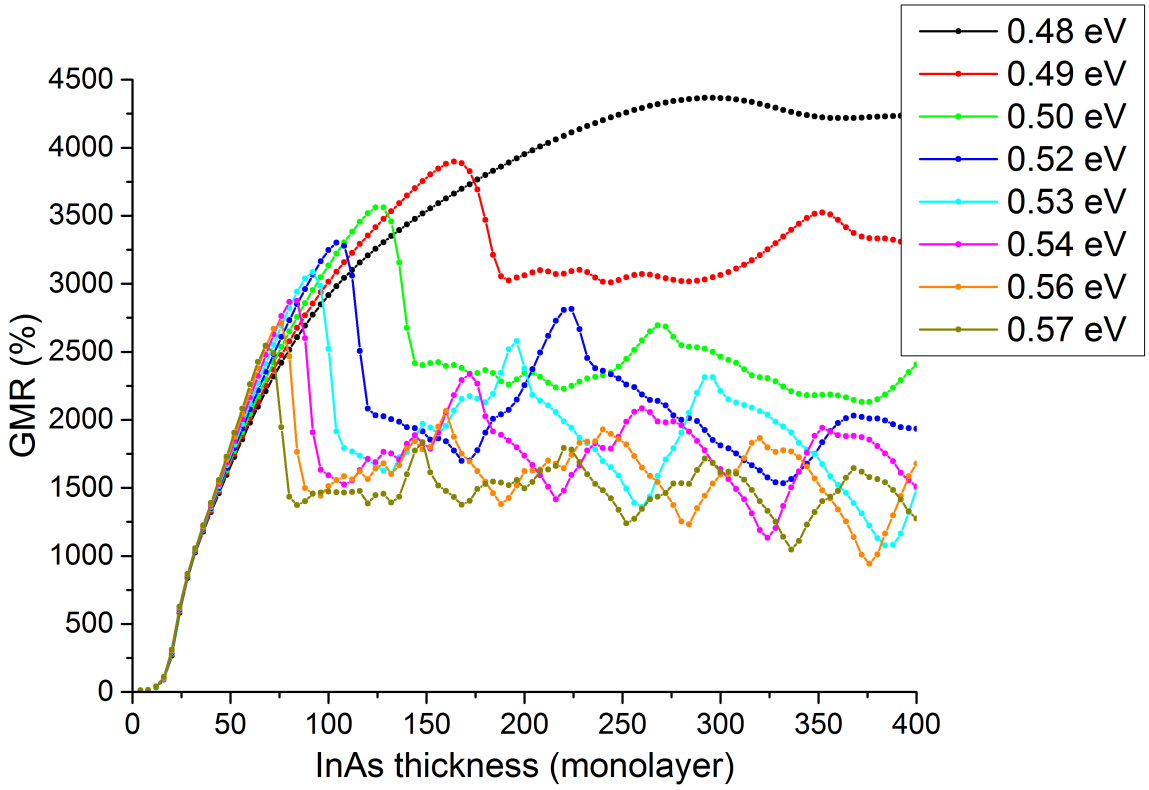

FIG. 4. GMR as a function of InAs thickness at various Fermi levels in the InAs conduction band

TABLE I. Comparison between average observed P_{InAs} from simulations to predicted P_{InAs} from Eq. (7) and (8).

$E_{f,InAs}$	0.490eV	0.503eV	0.517eV	0.531eV	0.544eV	0.558eV	0.571eV
Observed P_{InAs}	188	144	132	102	89	81	75
Calculated P_{InAs}	212	153	126	109	98	89	83

modulated by an envelope function. The Bloch function is derived from the bulk states at the band edge nearest to the Fermi level, and the envelope function ensures that the boundary conditions are met at the interfaces. This type of wave function originates from an expansion of the quantum-well wave function around the bulk states of the band edge, thus it's especially suitable to describe materials with Fermi level close to the band edge, for example, doped semiconductors as InAs in our system. The combination of the Bloch function with wave vector k_{edge} and its modulating envelope function with wave vector k_{env} gives rise to a total wave vector, i.e. the Fermi wave vector:

$$k_{tot} = k_f = k_{edge} \pm k_{env}. \tag{4}$$

Since the envelope function determines the overall amplitude of the wave function, when the thickness of the quantum well coincides with the peaks of the envelope, resonances are expected to occur and bring about an enhancement in transmission. Therefore, we expect an oscillation in conductance with a period P that is half of the wave length of the envelope function, that is:

$$P = \frac{\pi}{k_{env}}. \tag{5}$$

In the case of InAs, the band edge closest to the Fermi level is at the center of the 2D Brillouin Zone, thus $k_{edge,InAs} = 0$ and Eq. (4) becomes:

$$k_{f,InAs} = k_{env,InAs}. \tag{6}$$

(The bands are symmetric on the two sides of the center of the Brillouin Zone, so the $\pm$ sign doesnt make a difference.) Note that for the zinc blende lattice of InAs, the zone-boundary wave vector $k_{BZ,InAs} = 2\pi/a_{InAs} = \pi/2d_{InAs}$, where a_{InAs} is the lattice constant, and d_{InAs} is the spacing between adjacent atomic planes ($a_{InAs} = 4d_{InAs}$ for zinc blende lattice). If we choose d_{InAs} as the unit of the period in InAs (P_{InAs}), and $k_{BZ,InAs}$ as the unit of $k_{f,InAs}$, one then obtains from Eq. (5) and (6):

$$P_{InAs} = \frac{2}{k_{f,InAs}}. \tag{7}$$

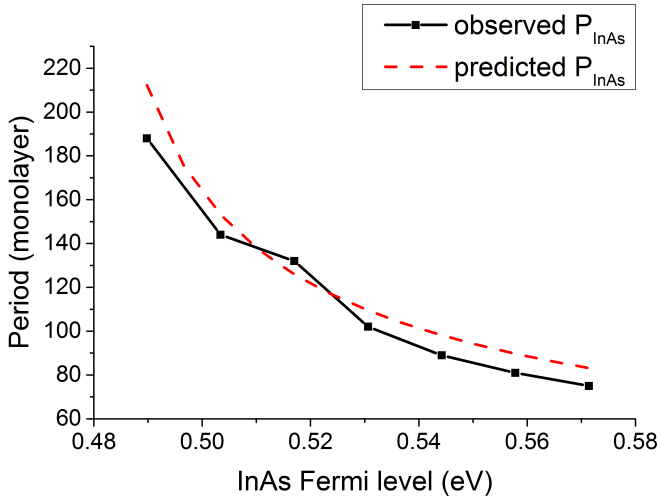

FIG. 5. Average observed P_{InAs} from simulations and predicted P_{InAs} from Eq. (7) and (8) as functions of the Fermi level position.

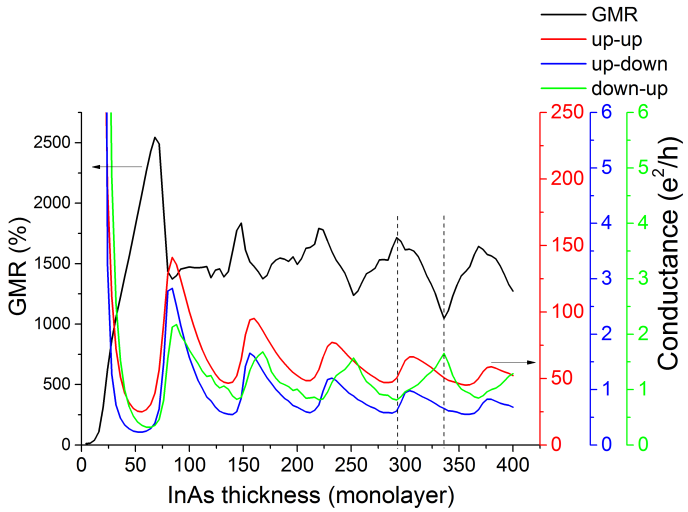

FIG. 6. GMR and conductances as functions of InAs thickness at Fermi level 0.57eV. The dashed lines are given as guides to the eye for one GMR peak and valley.

Since we are interested only in the region no more than a couple tenths of eV above the band edge, we can obtain an analytical expression of $k_{f,InAs}$ in terms of the Fermi energy $E_{f,InAs}$ by a parabolic approximation to the conduction band that we input to our simulations. This gives us:

$$k_{f,InAs} = \sqrt{\frac{E_{f,InAs} - 0.475(eV)}{166.62}} \quad \text{(in units of } k_{BZ,InAs}\text{)}. \tag{8}$$

Using Eq. (7) and (8), we are ready to calculate P_{InAs} in terms of $E_{f,InAs}$ and compare them to the average observed periods from simulations. The results are summarized in Table I and Fig. 5. It shows that the above equations can produce periods in close approximation of the ones observed, with errors no more than 10 monolayers (other than 0.49eV). Note that only the local maxima are used to identify the peak positions in simulation results. However, as can be seen from Fig. 4, some of these local maxima are biased towards the left of the whole shape of the peaks, and thus can be misleading in finding the actual peak positions. Also, the periods are fairly large. Considering these two factors both introduce errors to the observed periods, they are believed to be in reasonable agreement with the calculated periods. We therefore conclude that the model described above can truly explain the physical origin of the GMR oscillations with respect to InAs thickness.

One may argue that the above model is valid only for addressing the oscillatory conductance of one specific magnetization configuration in our system, but not necessarily the oscillatory GMR, since GMR is defined as the relative variation of the conductance between P and AP configurations. Therefore, it is necessary to examine how the conductance depends on InAs thickness as well. Fig. 6 shows a plot of GMR and conductance channels vs. InAs thickness corresponding to the situation of Fermi level at 0.57eV. The notion up-down conductance ($G_{\uparrow\downarrow}$) means the conductance of majority-spin electrons in the left Fe lead to the minority-spin band in the second Fe layer, and similar for the other notions. $G_{\downarrow\downarrow}$ is not shown because it is too small to have any visible effect on GMR. One immediately sees that the GMR oscillations and the conductance oscillations are in fact not in phase. However, the three conductance channels are almost in phase among themselves. Notice that although $G_{\downarrow\uparrow}$ seemingly shows a larger period (or a seemingly phase shift), this is actually not the case, as can be confirmed by the equal spacing between the oscillation valleys of the three conductance channels. Instead, $G_{\downarrow\uparrow}$ shows a transition of the peak shape from longer right tails to longer left tails. This transition of the $G_{\downarrow\uparrow}$ peak shape mostly controls the GMR oscillation: the GMR peaks are positioned at the $G_{\downarrow\uparrow}$ valleys, while the GMR valleys at the $G_{\downarrow\uparrow}$ peaks. Another feature shared by the conductances is that the peak values tend to decay with increasing InAs thickness. This feature also manifests itself in GMR. Since we assume clean interfaces and no defects in our simulations, the decay of the peaks cannot be explained by any mean-free path arguments. Rather, it should be explained by a cancellation effect among the partial conductances in the 2D Brillouin Zone around a stationary point of the perpendicular wave vector. (Indeed, the Γ point is a stationary point for InAs.) This argument is supported by a stationary-phase approximation to the 2D Brillouin Zone sum of the partial conductances[41], which is valid for large layer thickness, as is the case for InAs here.

To end our discussions of this section, we would like to point out that the GMR oscillation with respect to InAs thickness is a novel effect that has not been reported before. Unlike the common GMR oscillations observed in a

metallic spacer sandwiched between ferromagnetic layers, we have demonstrated a GMR oscillation in a semiconductor sandwiched by a ferromagnetic layer and a nonmagnetic layer. This GMR oscillation also provides us with the ability to tune the resistance of the system not only by changing the doping level of InAs, but also by changing the thickness of InAs, which, unlike changing doping, doesnt have to change GMR. Fig. 7 is a scatter plot of GMR vs. RA product of P configuration (RA_P) corresponding to Fermi level at 0.52eV. Clearly, GMR is not a monotonic function of the RA product, instead, for a given GMR, the RA product has various tunable values. For example, with a GMR of 2000%, the RA product can have values ranging from $10\,\Omega\,\mu m^2$ to $50\,\Omega\,\mu m^2$. Particularly, with merely 32 InAs monolayers (∼9nm), the system already shows a GMR of 1042% with an RA product of only $7.8\,\Omega\,\mu m^2$. In other words, with a $7.8\,\Omega$ resistance, the size of the scattering region can be as small as $1\mu m^2 \times 13nm$ (4 monolayers of Ag, 8 monolayers of Fe and 32 monolayers of InAs).

B. GMR dependence on Ag spacer thickness

In this section, we are going to examine the relation between GMR and Ag spacer thickness in Fe/Ag/Fe/InAs/Ag. The Fermi level of InAs was set to be 0.50eV and 0.56eV (both in the conduction band). The thickness of InAs was chosen close to the positions of the first peaks shown in Fig. 4 (120 monolayers for 0.50eV and 100 monolayers for 0.56eV). The resulting GMR as a function of the Ag thickness is plotted in Fig. 8. In Both cases, the GMR exhibit an oscillatory behavior with a period of 8 monolayers. This period is larger than the ones observed in experiments[15] or in other simulations[22,42], which are about 5 monolayers. Nonetheless, the explanation for this discrepancy is clear: the nearest neighbor treatment in our simulation causes slight distortion in the band structure of Ag. In fact, we can again use Eq. (4) and (5) to calculate the oscillation period for Ag (P_{Ag}). The band edge of Ag is at the zone boundary, so $k_{edge,Ag} = k_{BZ,Ag} = 2\pi/a_{Ag} = \pi/d_{Ag}$, where a_{Ag} is the lattice constant, and d_{Ag} is the atomic plane spacing ($a_{Ag} = 2d_{Ag}$ for FCC lattice). One then obtains:

$$P_{Ag} = \frac{1}{1 - k_{f,Ag}}, \tag{9}$$

where P_{Ag} is in units of d_{Ag} and $k_{f,Ag}$ in units of $k_{BZ,Ag}$. For the true Ag band structure, $k_{f,Ag} = 0.819 k_{BZ,Ag}$, thus Eq. (9) gives $P_{Ag} = 1/(1 - 0.819) = 5.5$ monolayers; whereas in the band structure that is input to our simulations with only nearest neighbor interactions, $k_{f,Ag} = 0.878 k_{BZ,Ag}$, so $P_{Ag} = 1/(1-0.878) = 8.2$ monolayers. The above discussion confirms that the slight distortion from the nearest neighbor treatment is indeed the reason for the difference between the oscillation periods. However, it also demonstrates that our calculation is self-consistent, and will not cause qualitative errors. Both cases in Fig. 8 shows GMR peaks above 1000%, but the peak values and the oscillation amplitudes are quite different from each other. When the Fermi level is closer to the InAs conduction band bottom (0.50eV), the peak GMR is larger and so is the oscillation amplitude (10% ∼ 4000% for 0.50eV compared to 350% ∼ 1500% for 0.56eV). This is because, in this situation, the electrons allowed to transmit are closer to the Γ point, imposing a stronger wave vector filtering effect that favors large GMR. Also, the Γ point is a stationary point of the perpendicular wave vector for Ag. When the region allowing transmission is smaller surrounding the stationary point,

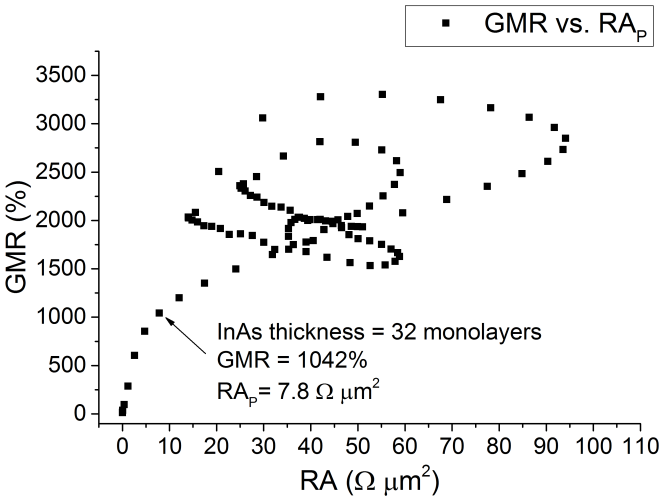

FIG. 7. GMR vs. RA product of P configuration with Fermi level at 0.52eV. The selected point is to demonstrate a situation with large GMR, small RA and small size of scattering region.

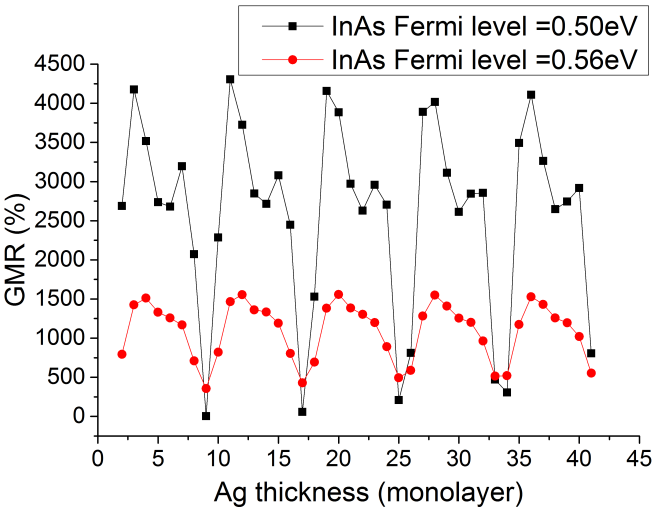

FIG. 8. GMR dependence on the Ag spacer thickness at two Fermi levels in the InAs conduction band.

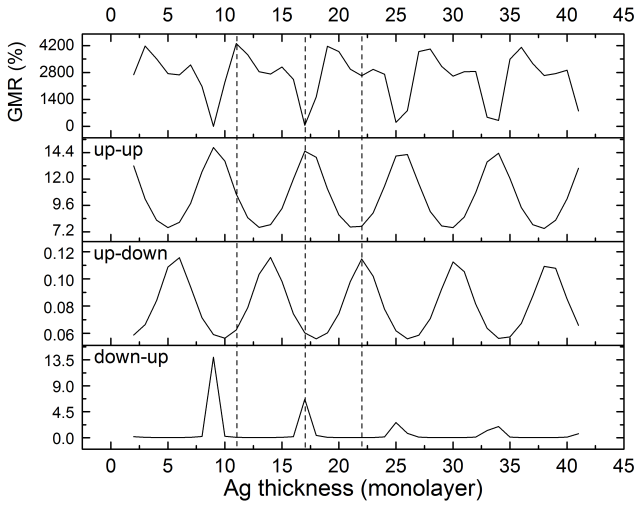

FIG. 9. GMR (top panel) and conductances (lower three panels) vs. Ag thickness with Fermi level at 0.50eV. Conductances are in units of e^2/h. Dashed lines are given as guides to the eye for one GMR peak, one GMR valley, and one small dip near GMR peak.

less partial conductances with periods different from the stationary period contribute to the total conductance, giving a stronger coherent interference and thus a larger oscillation amplitude. To study the phase shifts between GMR and different conductance channels with respect to Ag thickness, we plot the results in Fig. 9 for Fermi level at 0.50eV ($G_{\downarrow\downarrow}$ is not shown for its value is too small). The results are similar for 0.56eV. Interestingly, $G_{\uparrow\uparrow}$ and $G_{\downarrow\uparrow}$ are in phase with each other (and almost antiphase with $G_{\uparrow\downarrow}$), and they mostly determine the GMR. This is different from other simulations[42], where $G_{\uparrow\uparrow}$ and $G_{\downarrow\uparrow}$ are almost antiphase. According to Ref.[42] with the structure Fe/Ag/MgO/Fe, the Ag layer represents a potential step in the system and causes a phase shift between $G_{\uparrow\uparrow}$ and $G_{\downarrow\uparrow}$, which largely enhances the MR. It may be that the additional Ag layer that is introduced as the right lead in our system causes an additional phase shift, and as a result aligns the phase between $G_{\uparrow\uparrow}$ and $G_{\downarrow\uparrow}$. This phase alignment between the two dominating conductance channels in P and AP configurations obviously weakens the GMR enhancement. As a result, the $G_{\uparrow\uparrow}$ peaks don't align with the GMR peaks, but rather, with the GMR valleys; whereas the GMR peaks are positioned away from the $G_{\downarrow\uparrow}$ where $G_{\uparrow\uparrow}$ still has relatively large values. The $G_{\uparrow\downarrow}$ peaks, on the other hand, match with the small dips near the GMR peaks.

C. GMR dependence on the Fermi level position relative to the InAs bands

In this section, we present the simulation results of GMR and RA products (RA_P for P configuration and RA_{AP} for AP configuration) as functions of the Fermi level position for a wide range of energies, covering the region from the valence band top (0eV) to the conduction band bottom (0.47eV). During these simulations, the thicknesses of InAs, Fe and Ag are fixed to be 200, 8, and 4 monolayers respectively. The results are plotted in Fig. 10. We can see that GMR is enhanced to values above 1000% from 0.10eV to 0.64eV, ranging from the InAs band gap to the conduction band bottom. In this energy region, the RA_P peak and RA_{AP} peak are offset, giving rise to a large GMR. As discussed in Section III A, although InAs filters wave vectors towards the Γ point both in the band gap and at the conduction band bottom, the mechanisms of GMR enhancement are in fact of distinct natures. This is demonstrated by the RA products. When the Fermi level is in the InAs band gap, GMR is greatly enhanced, and the RA products are extremely large (due to the large thickness of InAs), indicating that InAs is an insulator favoring perpendicular tunneling. The RA products abruptly decrease as the Fermi level enters the InAs conduction band, indicating that InAs now operates as a conductor, but the GMR is still very large. In fact, the GMR peak on the right is inside the conduction band, which means that the wave vector filtering effect is stronger there than in the band gap, even with this large InAs thickness. As the Fermi level grows further into the conduction band, GMR and RA products both decrease, as more and more electrons far from the Γ point start to effectively transmit. However, there still exists an energy region where the GMR is above 1000% (larger than conventional GMR systems and comparable to conventional MTJs) with RA_P smaller than $10\,\Omega\,\mu m^2$ (orders of magnitude larger than conventional GMR structures and orders of magnitude smaller than

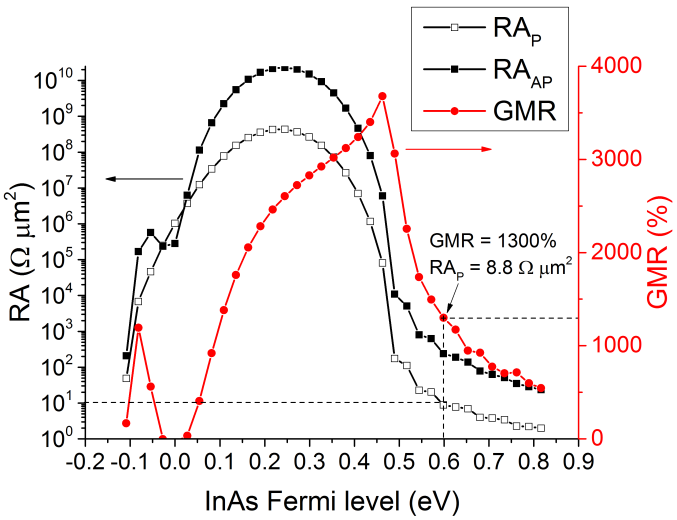

FIG. 10. GMR and RA products as functions of the Fermi level position. The valence band top is at 0eV and the conduction band bottom at 0.47eV. The dashed lines are guides to the eye for a selected point whose GMR is above 1000% and RA_P below $10\,\Omega\,\mu m^2$.

conventional MTJs). We have selected one of these cases and indicated it in Fig. 10. Another observation is that the offset between the RA_P and RA_{AP} peak gives rise to an inverse GMR effect near the top of the valence band, which only exists within less than a tenth of eV. With the Fermi level going further into the valence band, a relatively large GMR effect emerges again, as indicated by the smaller GMR peak on the left. This is because the top of the valence band, similar to the bottom of the conduction band, is confined around the Γ point, thus also imposing a wave vector filtering effect favoring perpendicular transmission and enhanced GMR. However, the spin-polarized Δ_1 states that dominate conductance are s-like, while the top of the InAs valence band is p-like, thus there exists a symmetry mismatch that weakens GMR. As can be seen in Fig. 10, the enhanced GMR in the valence band quickly vanishes as the Fermi level decreases.

IV. SUMMARY

We have presented a detailed study on the enhancement and oscillation of CPP GMR in the heterostructure Fe/Ag/Fe/InAs/Ag(100). Our calculations demonstrate that with optimal Ag and InAs thickness the system is able to achieve GMR higher than 1000%. This large GMR results from the coherent conduction of highly polarized Δ_1 states limited at the center of the 2D Brillouin Zone, which is due to the wave vector filtering effect imposed by the InAs layer. We show that GMR is an oscillatory function of Ag thickness with amplitude tuned by the InAs Fermi energy. And depending on the position of Fermi level, GMR either exhibits a saturation behavior (in the InAs band gap), or oscillates (in the InAs conduction band) with respect to InAs thickness. Although GMR oscillation with respect to nonmagnetic spacer thickness is a common phenomenon, it has only been observed in metallic spacer sandwiched between ferromagnetic layers. What we have shown in this article is a GMR oscillation in a semiconductor sandwiched between a nonmagnetic layer and a ferromagnetic layer, which is a novel phenomenon. Interestingly, despite the different natures of the spacer layers and the sandwiching layers, the GMR oscillations can be well explained by one single model of quantum-well state resonances and the oscillation periods are solely determined by the Fermi wave vector of the spacer layers in the perpendicular direction. We have shown that the calculated periods and the observed ones are in good agreement. The advantage of our proposed system is that its resistance is tunable by the Fermi level and the InAs thickness, and the RA product falls into the region between conventional GMR structures and MTJs. This feature enables our system to produce a large GMR and a detectable signal while maintaining a reasonably low resistance that scales nicely with decreasing device size, which is very desirable for nowadays technologies especially in high areal density magnetic recording. We have illustrated this feature by showing the dependence of GMR and RA product on a wide range of InAs Fermi energies. One specific configuration of our system with an RA product as low as $7.8\,\Omega\,\mu m^2$ and a GMR above 1000% has been demonstrated, and at the same time the scattering region is only 13nm long.

ACKNOWLEDGMENTS

This work was supported primarily by C-SPIN, one of the six SRC STARnet Centers, sponsored by MARCO and DARPA. We are also grateful to Tao Qu for useful discussions.

* victora@ece.umn.edu

[1] M. N. Baibich, J. M. Broto, A. Fert, F. Nguyen Van Dau, F. Petroff, P. Etienne, G. Creuzet, A. Friederich, and J. Chazelas, Phys. Rev. Lett. **61**, 2472 (1988).

[2] G. Binasch, P. Grünberg, F. Saurenbach, and W. Zinn, Phys. Rev. B **39**, 4828(R) (1989).

[3] J. Katine and E. E. Fullerton, J. Magn. Magn. Mater. **320**, 1217 (2008).

[4] J. Barnaś, A. Fuss, R. E. Camley, P. Grünberg, and W. Zinn, Phys. Rev. B **42**, 8110 (1990).

[5] W. P. Pratt, S.-F. Lee, J. M. Slaughter, R. Loloee, P. A. Schroeder, and J. Bass, Phys. Rev. Lett. **66**, 3060 (1991).

[6] T. Valet and A. Fert, Phys. Rev. B **48**, 7099 (1993).

[7] K. M. Schep, P. J. Kelly, and G. E. W. Bauer, Phys. Rev. Lett. **74**, 586 (1995).

[8] C. Yu, S. Li, W. Lai, M. Yan, Y. Wang, and Z. Wang, Phys. Rev. B **52**, 1123 (1995).

[9] F. Petroff, A. Barthélemy, D. H. Mosca, D. K. Lottis, A. Fert, P. A. Schroeder, W. P. Pratt, R. Loloee, and S. Lequien, Phys. Rev. B **44**, 5355(R) (1991).

[10] S. S. P. Parkin, R. Bhadra, and K. P. Roche, Phys. Rev. Lett. **66**, 2152 (1991).

[11] S. S. P. Parkin, N. More, and K. P. Roche, Phys. Rev. Lett. **64**, 2304 (1990).

[12] D. H. Mosca, F. Petroff, A. Fert, P. A. Schroeder, W. P. Pratt, and R. Loloee, J. Magn. Magn. Mater. **94**, L1 (1991).

[13] D. Edwards and J. Mathon, J. Magn. Magn. Mater. **93**, 85 (1991).

[14] Y. Wang, P. M. Levy, and J. L. Fry, Phys. Rev. Lett. **65**, 2732 (1990).

[15] J. E. Ortega, F. J. Himpsel, G. J. Mankey, and R. F. Willis, Phys. Rev. B **47**, 1540 (1993).

[16] T. Miyazaki and N. Tezuka, J. Magn. Magn. Mater. **139**, L231 (1995).

[17] W. H. Butler, X.-G. Zhang, T. C. Schulthess, and J. M. MacLaren, Phys. Rev. B **63**, 054416 (2001).

[18] J. Mathon and A. Umerski, Phys. Rev. B **63**, 220403(R) (2001).

[19] S. S. P. Parkin, C. Kaiser, A. Panchula, P. M. Rice, B. Hughes, M. Samant, and S.-H. Yang, Nature Materials **3**, 862 (2004).

[20] S. Yuasa, T. Nagahama, A. Fukushima, Y. Suzuki, and K. Ando, Nature Materials **3**, 868 (2004).

[21] S. Ikeda, J. Hayakawa, Y. Ashizawa, Y. Lee, K. Miura, H. Hasegawa, M. Tsunoda, F. Matsukura, and H. Ohno, Appl. Phys. Lett. **93**, 082508 (2008).

[22] G. Autès, J. Mathon, and A. Umerski, Phys. Rev. B **83**, 052403 (2011).

[23] H. Ohno, K. Yoh, T. Doi, A. Subagyo, K. Sueoka, and K. Mukasa, J. Vac. Sci. Technol. B **19**, 2280 (2001).

[24] L. Ö. Olsson, C. B. M. Andersson, M. C. Håkansson, J. Kanski, L. Ilver, and U. O. Karlsson, Phys. Rev. Lett. **76**, 3626 (1996).

[25] C. Ohler, C. Daniels, A. Förster, and H. Lüth, J. Vac. Sci. Technol. B **15**, 702 (1997).

[26] B. Feng, S. Huang, J. Wang, D. Pan, J. Zhao, and H. Q. Xu, J. Appl. Phys. **119**, 054304 (2016).

[27] A. Razavieh *et al.*, ACS Nano **8**, 6281 (2014).

[28] D. A. Papaconstantopoulos, *Handbook of the Band Structure of Elemental Solids* (Plenum, New York, 1986).

[29] J.-M. Jancu, R. Scholz, F. Beltram, and F. Bassani, Phys. Rev. B **57**, 6493 (1998).

[30] W. A. Harrison, *Electronic Structure and the Properties of Solids* (Dove, New York, 1989).

[31] D. S. Fisher and P. A. Lee, Phys. Rev. B **23**, 6851(R) (1981).

[32] S. Sanvito, C. J. Lambert, J. H. Jefferson, and A. M. Bratkovsky, Phys. Rev. B **59**, 11936 (1999).

[33] J. Velev and W. Butler, J. Phys.: Condens. Matter **16**, R637 (2004).

[34] D. J. Thouless and S. Kirkpatrick, J. Phys. C **14**, 235 (1981).

[35] A. MacKinnon, Z. Phys. B **59**, 385 (1985).

[36] F. Sols, M. Macucci, U. Ravaioli, and K. Hess, J. Appl. Phys. **66**, 3892 (1989).

[37] K. Kazymyrenko and X. Waintal, Phys. Rev. B **77**, 115119 (2008).

[38] C. H. Lewenkopf and E. R. Mucciolo, J. Comput. Electron. **12**, 203 (2013).

[39] D. K. Ferry and S. M. Goodnick, *Transport in Nanostructures* (Cambridge University Press, Cambridge, U.K., 1997).

[40] J. Mathon and A. Umerski, Phy. Rev. B **74**, 140404(R) (2006).

[41] J. Mathon, M. Villeret, and H. Itoh, Phys. Rev. B **52**, R6983(R) (1995).

[42] G. Autès, J. Mathon, and A. Umerski, Phy. Rev. B **80**, 024415 (2009).